

Article

A Combined IR-GPS Satellite Analysis for Potential Applications in Detecting and Predicting Lightning Activity

Leo Pio D'Adderio ¹, Luigi Pazienza ¹, Alessandra Mascitelli ^{2,3} , Alessandra Tiberia ¹  and Stefano Dietrich ^{1,*} 

¹ CNR-ISAC, Consiglio Nazionale delle Ricerche, Roma, Via del Fosso del Cavaliere 100, 00133 Roma, Italy; leopio.dadderio@artov.isac.cnr.it (L.P.D.); lu.pazienza@gmail.com (L.P.); alessandra.tiberia@artov.isac.cnr.it (A.T.)

² Sapienza Università di Roma, DICEA, Via Eudossiana 18, 00184 Roma, Italy; alessandra.mascitelli@uniroma1.it

³ Politecnico di Milano, DICA - GEOlab, Piazza Leonardo da Vinci 32, 20133 Milano, Italy

* Correspondence: s.dietrich@isac.cnr.it; Tel.: +39-06-49934575

Received: 18 February 2020; Accepted: 19 March 2020; Published: 23 March 2020



Abstract: Continuous estimates of the vertical integrated precipitable water vapor content from the tropospheric delay of the signal received by the antennas of the global positioning system (GPS) are used in this paper, in conjunction with the measurements of the Meteosat Second Generation (MSG) spinning enhanced visible and infrared imager (SEVIRI) radiometer and with the lightning activity, collected here by the ground-based lightning detection network (LINET), in order to identify links and recurrent patterns useful for improving nowcasting applications. The analysis of a couple of events is shown here as an example of more general behavior. Clear signs appear before the peak of lightning activity on a timescale from 2 to 3 h. In particular, the lightning activity is generally preceded by a period in which the difference between SEVIRI brightness temperature (TB) at channel 5 and channel 6 (i.e., ΔTB) presents quite constant values around 0 K. This trend is accompanied by an increase in precipitable water vapor (PWV) values, reaching a maximum in conjunction with the major flash activity. The results shown in this paper evidence good potentials of using radiometer and GPS measurements together for predicting the abrupt intensification of lightning activity in nowcasting systems.

Keywords: lightning; convection; radiometer; GPS; brightness temperature; zenith total delay; precipitable water vapor

1. Introduction

Lightning is a natural phenomenon studied since the second half of the 18th century due to its practical and scientific interest. If the practical aspect is mainly represented by the necessity of granting the security of people, aircrafts, and buildings, the scientific interest for a better understanding of the physics of the atmosphere is always actual. The statistical nature of the discharge mechanism, combined with difficulties in making direct measurements inside thunderstorms, make them one of the most familiar natural phenomena remaining relatively poorly understood. Technological improvements in ground measurements and remote sensing methods are now providing new insights.

The exact conditions under which the electrical breakdown in air will take place it is not exactly predictable. The distribution and motion of thunderstorm electric charges, most of which reside in hydrometeors (liquid or frozen water particles), are complex and change continuously as the cloud

evolves. Several theories have been proposed to explain charge generation and separation inside clouds. In general, they involve microphysical processes for different water phases [1].

A well-established theory explaining cloud electrification is known as the non-inductive precipitation charging mechanism [2]. It is based on the experimental observation that a charge transfer occurs when ice crystals collide with graupel particles in the presence of water droplets [2–5]. The magnitude of the electric charge created during collisions depends on a number of factors like: cloud water content, ice crystal size, relative velocity of particles, and chemical contaminants in water and droplet size. On the other hand, in understanding the lightning initiation, tropospheric water vapor variations inside clouds represent a key element. However, monitoring its variations over time is very difficult. Recently, some experimental field campaigns taking advantage of combined ground radar and lightning measurements showed that most of the flashes originate in regions with a high concentration of small rimed particles or hail [6]. In particular, it was found that a good predictor of lightning activity and intensity is the altitude of the rimed particle column [7].

The ascending air currents transport aloft water vapor. The stronger the updraft, the thicker the clouds, and the greater the number of particles that are transported to the upper cloud levels. The volume of water carried upwards, in addition to indicating the intensity of the convection, influences the electrification processes.

Evident correlations between lightning activity and upper tropospheric water vapor (UTWV) were found by some researchers [8]. They found a good agreement between long-term measurements of UTWV and extremely low frequency (ELF: $1\text{Hz} < f < 100\text{Hz}$) data, showing that the maximum and minimum ELF often precede the maximum and minimum of water vapor on a daily basis.

The possibility to monitor precipitable water vapor using the global positioning system (GPS) was first explored by [9,10], while others [11] proposed meteorological applications of GPS measurements on numerical prediction for meteorological models.

The correlation between the increase in atmospheric water vapor and intense rainfall events was investigated [12]. Precipitable water vapor estimates from GPS were evaluated for intense rainfall events observed by an X-band radar during the CHUVA campaign in Brazil, showing important spikes in measurements that precede the more intense rainfall events on a timescale from 30 to 60 min [12]. Currently the international scientific community is still investigating these issues and the results are particularly encouraging [13–15].

A statistical approach that combines integrated precipitable water vapor data from a GPS receiver with other meteorological data was first proposed by some researchers [16]. With the goal to find features able to predict lightning, they introduced a lightning index, which showed a marked trend anomaly up to about 12.5 h before the first lightning strike.

The purpose of this work is to analyze the presence and the number of lightning strokes during the different phases of some severe convective events, relating them to the brightness temperatures measured by satellite infrared sensors, and with the water vapor derived from GPS measurements.

Recently the term “lightning jump” has been coined to indicate the moment of development of a storm when the number of electric discharges increases in a very short time. This indicator is quite easy to extract both from the data provided by ground lightning networks [17] and, even better, from the data acquired by instruments embarked on a satellite such as the Geostationary Operational Environmental Satellite (GOES)-R geostationary lightning mapper (GLM) [18].

The joint use of lightning and observable radars has paved the way for nowcasting applications in which the lightning jump is the precursor of a few tens of minutes on the occurrence of strong hailstorms or very intense local rainfall [18,19]. The definition of reliable precursors of the lightning jump would allow to further anticipate the warnings that can be produced by the nowcasting systems.

This is the reason why the ultimate goal of the analysis in the paper is to investigate the possibility of using precipitable water vapor (PWV) in combination with brightness temperature (TB) to predict the lightning activity during a convective event.

The paper is organized as follows: in Section 2, the instrumentation is described, while the results of the analysis of the two case studies, selected among the numerous ones investigated, are discussed in Section 3. The last section reports the conclusions.

2. Instrumentations and Methods

In this study, the data collected by the lightning detection network (LINET) [20,21], the spinning enhanced visible and infrared imager (SEVIRI) radiometer, and the global navigation satellite systems (GNSS) were analyzed. In particular, a number of case studies have been investigated and two of them are shown.

2.1. LINET

The LINET network is a ground-based lightning detection system managed by nowcast GmbH. The LINET measuring stations are widely distributed over Europe and cover the entire Italian territory and the surrounding seas. Each LINET station has an antenna to detect very low frequency (VLF) and low frequency (LF) waves emitted during the flash, a GPS clock, a technical module (amplifier, filter, analog to digital converter), and a transmitter. The frequency ranges used allow LINET to detect both cloud-to-ground (CG) and intra-cloud (IC) lightning, even if these two signals have a wide overlapping range of emissions. The detection of the flashes is based on a pseudo-3D algorithm, characterized by 3 steps [20,21]. The ability of the pseudo-3D algorithm in evaluating the height of the starting breakdown is possible if the flash happens within 100 km from the antenna, which means that two LINET stations must not be at more than 200 km from each other to detect the same event with the appropriate efficiency [21]. The pseudo-3D algorithm is based on the following three main steps:

- 2D location of the flash through a time of arrival algorithm (TOA)
- Exploitation of the time delay at the sensor nearest to the lightning
- Time relaxation of the travel path of the radio-wave

The 2D location is possible thanks to the high-precision GPS clock equipped on each station. It is, in fact, the difference in the arrival times of the signal at the three or four receiving antennas that allows to determine the position of the lightning. Figure 1 shows what is above explained.

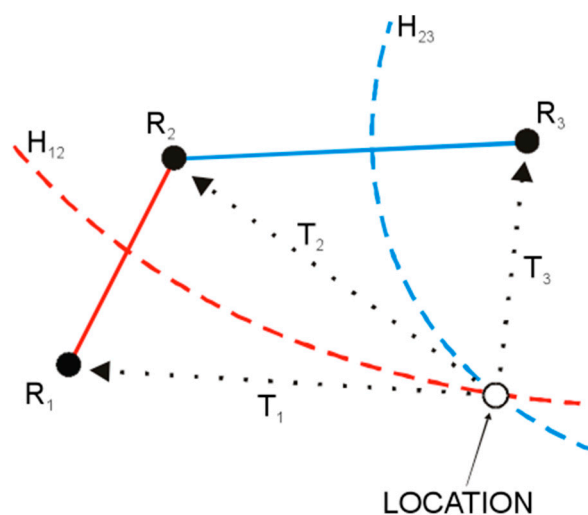


Figure 1. TOA algorithm estimate of the stroke's coordinates.

After locating the flash, the algorithm considers the delay between the source of the lightning and the nearest station: the bigger the delay, the more probable the flash is an IC rather than a CG. Lastly, the time relaxation of the travel path is used to estimate the height of the discharge.

2.2. SEVIRI

The most probable and accepted charging mechanism of the clouds is the riming electrification mechanism [2]. It is reasonable to expect that light ice crystals should be brought upward by the convective movements inside the cloud, while heavier graupel would occupy lower height inside the cloud structure. Aiming at the purpose of monitoring the cloud properties, the SEVIRI radiometer [22] has been used in this study. SEVIRI is one of the three payloads onboard the meteosat second generation (MSG) satellite. MSG has a geostationary orbit to continuously observe the full disk of Europe and Africa. SEVIRI is a scanning radiometer which captures a view of the Earth disk every 15 min. The scanner has an aperture of 50 cm and twelve channels from the infra-red to visible spectrum fulfilling the aim of high-quality data collection to be used for multiple purposes (i.e., as starting conditions for numerical weather prediction models, as cloud cover monitoring, etc.). SEVIRI's main product is the brightness temperature (TB) of the bodies observed during the scanning. According to Table 1, the channels used by the radiometer had been built to mainly analyze the cloud properties and specific atmospheric gases like CO₂ and Ozone.

Table 1. Spinning enhanced visible and infrared imager (SEVIRI)'s channels characteristics. Other than channel number and name, the central, minimum, and maximum wavelength (λ_{cen} , λ_{min} , and λ_{max} , respectively) are reported, as well as the main gas absorber.

Channel Number	Name	λ_{cen} (μm)	λ_{min} (μm)	λ_{max} (μm)	Main Gas Absorber	Main Gas Absorber
1	VIS 0.6	0.635	0.56	0.71	Window	Cloud detection
2	VIS 0.8	0.81	0.74	0.88	Window	Cloud detection
3	NIR 1.6	1.64	1.50	1.78	Window	
4	IR 3.9	3.90	3.48	4.36	Window	
5	WV 6.2	6.25	5.35	7.15	Water Vapor	
6	WV7.3	7.35	6.85	7.85	Water Vapor	
7	IR 8.7	8.70	8.30	9.10	Window	
8	IR 9.7	9.66	9.38	9.94	Ozone	
9	IR 10.8	10.80	9.80	11.80	Window	
10	IR 12.0	12.0	11.0	13.0	Window	
11	IR 13.4	13.40	12.40	14.40	Carbon dioxide	
12	HRV	Broad channel (about 0.4–1.1)			Window/Water Vapor	

Parallax correction was applied for this study to the SEVIRI data. Among the available SEVIRI channels, the IR channels 5, 6, and 9 have been used (respectively 6.25, 7.35, and 10.80 μm). In particular, the wavelengths at 6.25 and 7.35 μm were centered in the emission spectrum of the water vapor (WV). While the two WV channels (channels 5 and 6), other than to determine the water vapor distribution in two distinct layers of the atmosphere, can give an indication about the cloud optical depth, the IR channel 9 provides continuous observation of the cloud top temperature. A more detailed description of the SEVIRI channels can be found in a previous report [22].

2.3. GPS

The other technology employed in this research, in order to obtain a data comparison, is the global navigation satellite systems (GNSS).

Today, indeed, this system is used not only for navigation purposes, but also in many other fields like different monitoring applications [23,24], seismology [25,26], meteorology [15,27] and gravimetry [28]. In each context, GNSS signals are processed in order to obtain data able to improve the knowledge in terms of positions, velocities, accelerations, and quantities related to signal interactions in the satellite–receiver path.

Actually, during the satellite–receiver path, the interaction of GPS signals with the atmosphere content (dry air, moisture, and ions) causes a time delay of the signal propagation, which, multiplied

by the vacuum speed of light, results in an extra-distance with respect to the geometrical one. Characterizing the atmosphere by the way radio waves are propagated leads to its subdivision in ionospheric and tropospheric layer, where the ionosphere, the upper part of the atmosphere, is a dispersive medium and the troposphere is nondispersive [29]. In this sense, by applying the ionosphere-free combination [30] during the data processing, it is possible to exploit this property to obtain the part of the delay due to the troposphere, which is currently expressed in zenith total delay (ZTD) that is the delay related to each receiver along the zenith direction [30].

In this study, the signals from GPS constellation satellites have been used to estimate the amount of ZTD [29] and, consequently, the precipitable water vapor (PWV) [10].

To do this, a post-processing precise point positioning (PPP) [31] was carried out by “RTKLIB: An Open Source Program Package for GNSS Positioning” [32], which allowed to obtain ZTD estimations with a time rate of 30 s. Processing ancillary products were ephemeris and clocks provided by the Center for Orbit Determination in Europe (CODE).

ZTD measurements consist of two delay components, the zenith hydrostatic delay (ZHD) and the zenith wet delay (ZWD), expressed by the following equation:

$$ZTD = ZHD + ZWD \quad (1)$$

where the ZHD can be easily modeled through standard atmosphere models, while the ZWD is more variable and difficult to be estimated.

The wet component (ZWD) is linked to the presence of water vapor in troposphere and therefore more closely related to the meteorological topic.

European Centre for Medium-Range Weather Forecasts (ECMWF) reanalysis [33] data have been used to obtain the initial pressure (P) and temperature (T) data, starting from which, after appropriate adjustments, related to the difference in altitude between meteorological data and GPS receivers [14,34,35], it is possible to obtain ZWD values, from ZTD and ZHD values. Indeed, once ZTD, P, and T are available, the ZHD and, by difference, the ZWD, can be calculated. Then, by applying the procedure described previously [9], PWV can be computed.

At this point, a complete dataset of ZTD and PWV can be obtained for each day of interest and each receiver.

In particular, two geodetic receivers were involved in the study described in this paper. The first one is the so called RSTO (lon = 14.00148, lat = 42.65838, h = 102.6), which is part of the RING network (GPS National Integrated Network by the National Institute of Geophysics and Volcanology); this geodetic device is referred to the Pineto event of 2nd September 2018.

The other one is the so called NAPO (lon = 14.27598, lat = 40.87002, h = 127.7), part of the Campania Region Permanent Network and referred to the Naples event of 5th September 2015.

3. Results and Discussion

In this section, we will present two case studies in which PWV and TB measurements were analyzed together with lightning strokes recorded during the events. The considered storms occurred on 5th September 2015 over Naples and 2nd September 2018 over Pineto, respectively on the southwestern and centraleastern coast of Italy.

The purpose of the analysis was to identify the existence of a relationship among PWV, TB, and total lightning activity (i.e., IC + CG activity). It should be pointed out that PWV values estimated from the local GPS signal, especially when there was the passage of atmospheric disturbances, are representative measures only for a limited area around the antenna’s location (i.e., within 25 km from the GPS antenna). It is also worth mentioning that since the GPS processing software used a Kalman filter to initialize the system, the first two hours of PWV data have very low reliability and should not be considered.

3.1. Naples, 5th September 2015

In the storm observed on 5th September 2015, a convective cell was generated over the Tyrrhenian Sea, which then moved eastwards, hitting the city of Naples from approximately 7:30 to 10:30 UTC. An intense lightning activity was registered during the entire evolution of the event with more than 37,000 strokes detected by LINET in 5 h, with a very intense hailstorm with record-sized hailstones [36].

Figure 2 illustrates the evolution of the convective cell, taking into consideration four successive time intervals far one hour or slightly more from each other.

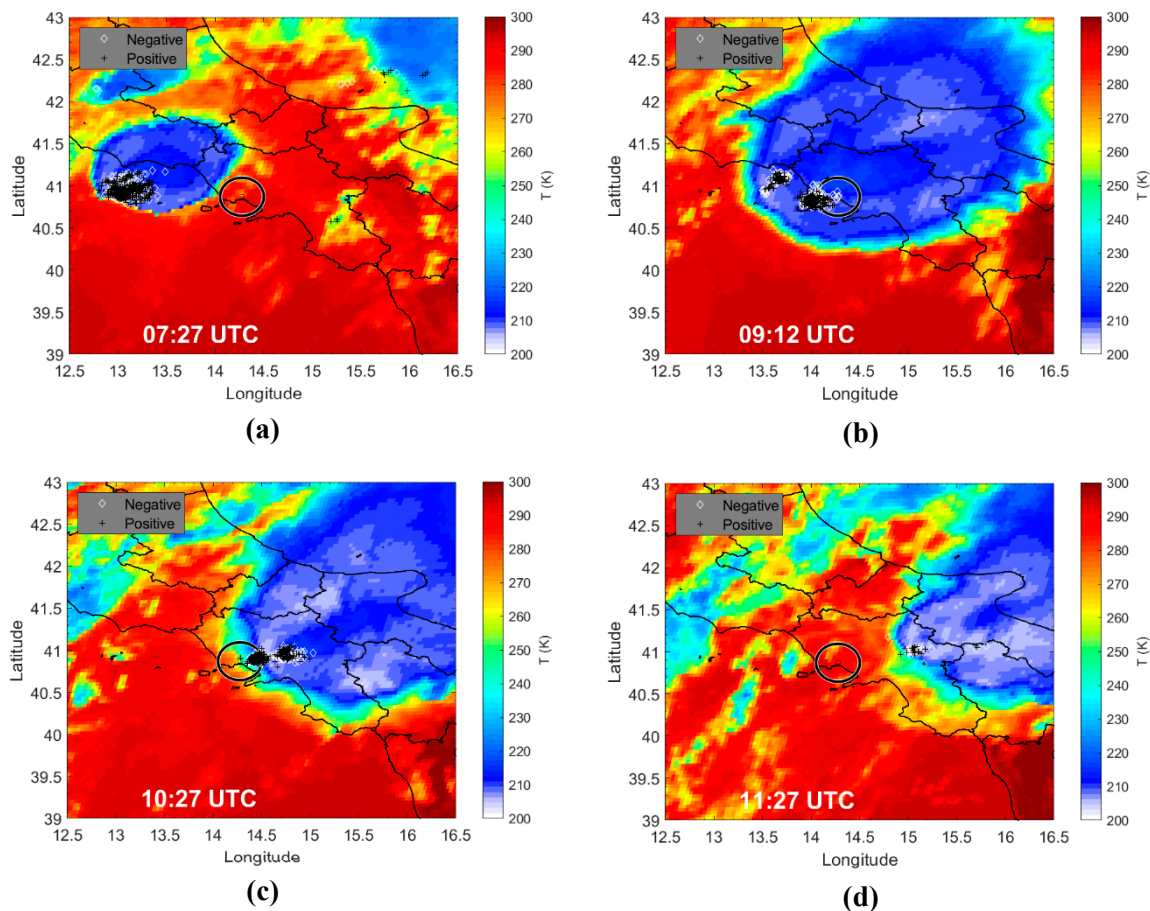


Figure 2. Time evolution of the convective cell hitting the Naples area on 5th September 2015. The panels (a) to (d) report the brightness temperature (TB) as measured by SEVIRI channel 9 and the positive (black crosses) and negative (white diamonds) strokes as recorded by the LINET network at (a) 07:27, (b) 09:12, (c) 10:27, and (d) 11:27 UTC, respectively. The black circle is centred in correspondence of GPS antenna and identifies the area where its measurements are consistent (i.e., around a 25-km radius).

The single panel shows the images of the TBs of channel 9 of the SEVIRI (TB_{ch9}) with superimposed lightning strokes, both positive (black crosses) and negative (white diamonds), recorded by the LINET network. Figure 2a shows the initial stage of the event at 07:27 UTC, with the active core of the cell (with $TB_{ch9} < 220$ K) on the sea, while the anvil already covered the south of the Lazio region and partially the northern part of the Campania region. Intense lightning activity is evidenced by a large number of both positive and negative strokes on the edge of the cell in the updraft region. During the mature phase of the event, the panel in Figure 2b, the event covers a huge spatial extension (approximately $2.5^\circ \times 3^\circ$) and very low TB_{ch9} values (i.e., approximately 210 K). The lightning activity takes place in two clearly distinct areas, one interesting the GPS antenna area and one further to the northwest. At 10:27 UTC (Figure 2c), the western edge of the convective cell is still affecting, albeit partially, the area of the GPS antenna, with lightning activity is still present. The panel in Figure 2d

shows the final stage of the event with the convective cell moved eastward from Naples, and with the lightning activity now negligible. Figure 2 evidences that both positive and negative lightning strokes are located at the edge of the low TBs' area, where evidently the strongest updraft takes place, triggering the lightning charging mechanism.

Figure 3 shows the hourly trend of the IC/CG ratio and the total lightning strokes detected during the storm evaluated over the $1^\circ \times 1^\circ$ box centred on the position of the GPS antenna. Moreover, the vertical grey dashed lines simply identify the time interval of interest (i.e., the time interval when the storm overpassed the measuring site), while the horizontal red dashed line represents the mean value of the IC/CG ratio over the same $1^\circ \times 1^\circ$ box for seven years, from 2012 to 2018.

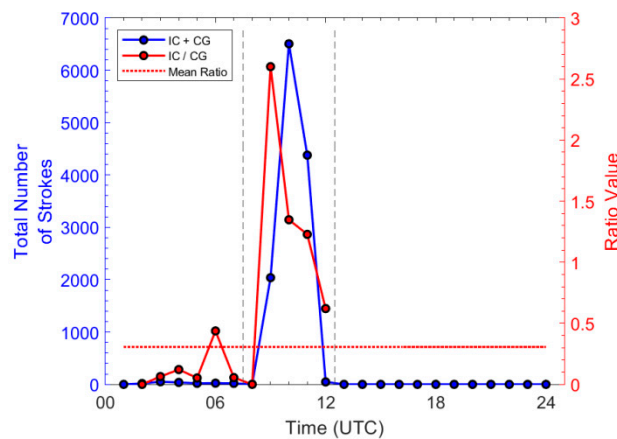


Figure 3. Hourly trend of the intra-cloud (IC)/cloud-to-ground (CG) ratio (solid red line) and total number of strokes (blue line) on 5 September 2015, over a $1^\circ \times 1^\circ$ box centred on the GPS antenna. The horizontal red dashed line represents the mean value of the IC/CG ratio over the same $1^\circ \times 1^\circ$ box for seven years from 2012 to 2018.

During this event, the IC/CG ratio shows two peaks, one at 06:00 UTC and one at 09:00 UTC. Actually, the peak at 06:00 UTC occurred with a total number of strokes lower than 100, so it is not meaningful of a strong IC activity. On the other hand, the peak at 09:00 UTC has been reached over a sample of about 2000 strokes and its value, slightly higher than 2.5, evidences the prevalence of IC with respect to CG strokes. Furthermore, the IC/CG ratio is about 9 times greater when compared with the IC/CG ratio mean value over the seven year dataset. Although the IC/CG ratio is mostly higher than 1 (except at 12:00 UTC), highlighting the prevalence of IC strokes, the peak of the IC/CG ratio precedes the peak of the maximum lightning activity (i.e., the IC/CG ratio peak occurred at 09:00 UTC, while the maximum number of strokes occurred at 10:00 UTC). Two possible explanations can be given for this temporal mismatch:

- ICs are easier to be triggered than CGs, especially at the beginning of the cell's lightning activity, because the path to be ionized is generally shorter.
- The presence of a LINET station in Naples certainly guarantees an optimum ability of detecting IC lightning strokes in the area of the considered event.

Of the two possible explanations, the second seems preferable since the cloud begins to become electrically active already at the moment of its formation over the sea. Moving towards the coast and approaching the LINET sensor in Naples, a greater number of IC is detected by the network.

We now want to discuss the possible relationship existing among PWV, TB, and lightning in order to investigate whether the first two quantities can be used as predictors of lightning activity. In this regard, Figure 4 shows the daily trend of PWV (blue line), of TB_{ch9} (red line), of the difference between TB measured by SEVIRI channel 5 and 6 (ΔTB —dotted point light blue line), and of total lightning (black line).

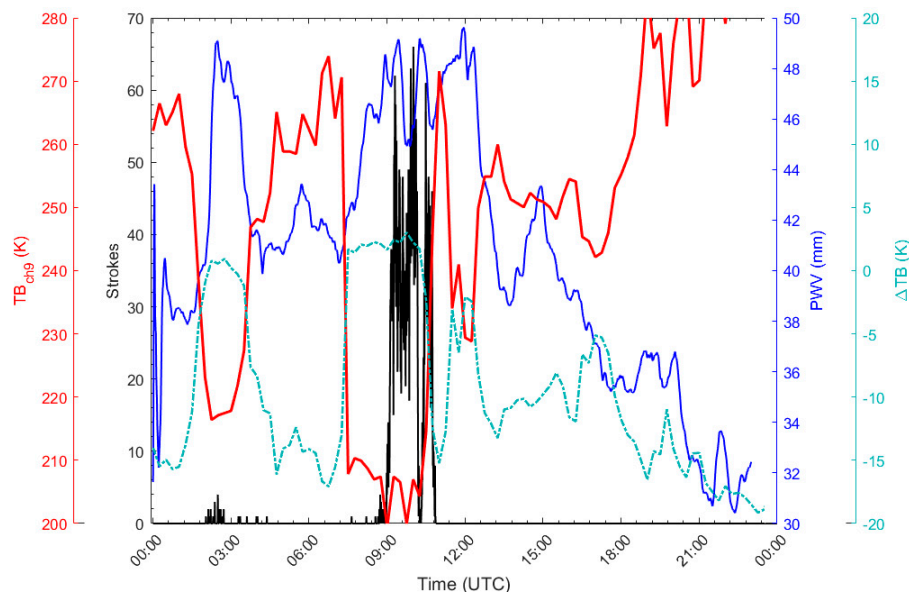


Figure 4. Trend of total number of strokes (black line), precipitable water vapor (PWV) (blue line), TB_{ch9} (red line), and ΔTB (dashed sky blue line) for the whole day of 5th September 2015 over the Naples area.

TB_{ch9} values reported in Figure 4 are the minimum values measured by SEVIRI at each acquisition (i.e., every 15 min) within 25 km from the GPS antenna. On the other hand, ΔTB is calculated as the difference between the mean values of channel 5 and 6 over a 3x3 pixels area centered over the GPS antenna. While the TB_{ch9} is intended to give an idea about the vertical extension of the convective cell (i.e., the colder the TB_{ch9} , the higher the cloud top), ΔTB gives an indication of the water vapor distribution along the air column and it is expected to have a trend comparable to PWV.

There are two peaks of PWV which both coincide with a minimum for the TB_{ch9} and higher values of ΔTB : the first peak is observed in coincidence with the small lightning activity around 02:30 UTC, while the second one is observed around 8:00 UTC, preceding of about one hour the greater lightning activity starting at 09:00 UTC. As expected, ΔTB has the same trend as the PWV (i.e., the PWV maxima/minima correspond to the ΔTB maxima/minima) and reaches zero or even positive values in correspondence of the maxima. It has to be highlighted that ΔTB has generally negative values in clear sky since SEVIRI channel 5 peaks at a higher altitude (about 350 hPa) than SEVIRI channel 6 (about 500 hPa). TB_{ch9} has a specular trend with respect to both PWV and ΔTB : it reaches its minimum values in coincidence with the lightning activity registered at 02:30 UTC and at 09:00 UTC. While for the first peak (i.e., 02:30 UTC), the timing of TB_{ch9} starting decreasing is the same as that of ΔTB and PWV starting increasing, this is not true for the second peak at 09:00 UTC. In this case, PWV starts increasing when ΔTB has already reached its maximum values (around 3 K at 07:30 UTC—it remains roughly constant until 10:00 UTC), and TB_{ch9} its minimum value (around 210 K at 07:30 UTC—it shows local depression around 200 K). A third PWV peak occurred at 12:00 UTC corresponding to a local minimum and maximum of TB_{ch9} and ΔTB , respectively. In particular, ΔTB does not reach positive values and no lightning activity is associated.

Figure 4 allows to appreciate the trend characteristics of the variables ZTD, TB, and ΔTB , also in relation to the evolution of lightning activity. The following Figures 5 and 6 try to investigate other relationships. The first attempt relates the intensity and polarity of the electric current of each electric discharge with the ZTD value measured at that moment (Figure 5).

The results show that negative strokes have higher current intensity values, as there are several negative strokes exceeding -20 kA, and reaching a maximum negative intensity close to -70 kA. On the other hand, positive discharges are the majority with the 60.1% of the total detected lightning strokes, but their intensity does not exceed 20 kA (except for some strokes). The 60.1% of positive

strokes are well above the 42.4%, which are the average percentage value of positive strokes detected in the same area over seven years of data examined (from 2012 to 2018). However, it is also interesting to note that the comparison with the long-term data series highlights the predominance of positive strokes during heavy convective rainfall. Nevertheless, the analysis does not show any particular range of PWV associated to positive or negative strokes, with both polarities registered for a PWV equal or greater of 45 mm.

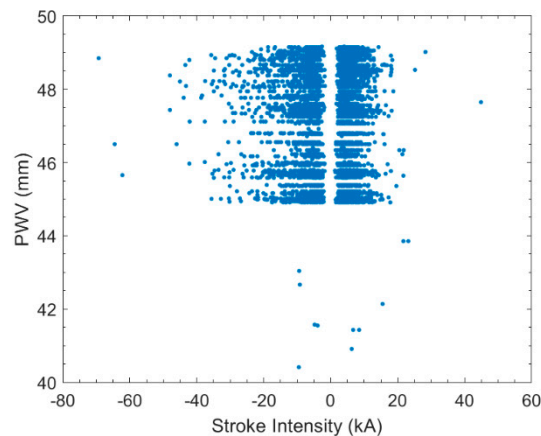


Figure 5. Scatterplot of PWV as a function of strokes intensity.

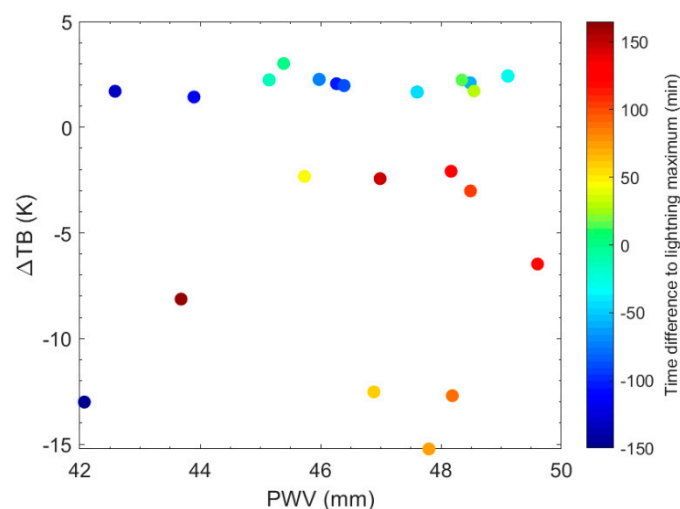


Figure 6. Scatterplot of ΔTB with respect to PWV as a function of time difference with respect to the main lightning activity.

Figure 6 relates the ΔTB (difference between SEVIRI channels 5 and 6) values with the PWV estimated with the GPS, taking into account the time difference with respect to the moment of maximum lightning activity (in this case study with respect to 10:00 UTC). The results show two clusters of points, with those following the maximum lightning activity (colored from yellow to red) mainly grouped in the region with a ΔTB lower than -2 K, while the points preceding up to 100 min the maximum lightning activity (colored from light blue to blue) have ΔTB values generally greater than 0 K. While this latter cluster is well identified with a limited spread of ΔTB values, the former (the points following the maximum lightning activity) shows a wide spread of ΔTB with values between -2 k and -15 K.

3.2. Pineto, 2nd September 2018

On 2nd September 2018, a violent storm occurred over the Central Italy, mainly involving the Adriatic coast and hitting the small town of Pineto for about five hours (between about 12:00 UTC

and 17:00 UTC). During the event, a heavy hailstorm caused damages to cars and structures. The storm presents very different characteristics compared to the Naples case study. Figure 7 illustrates the evolution of the convective cell, taking into consideration four successive time intervals.

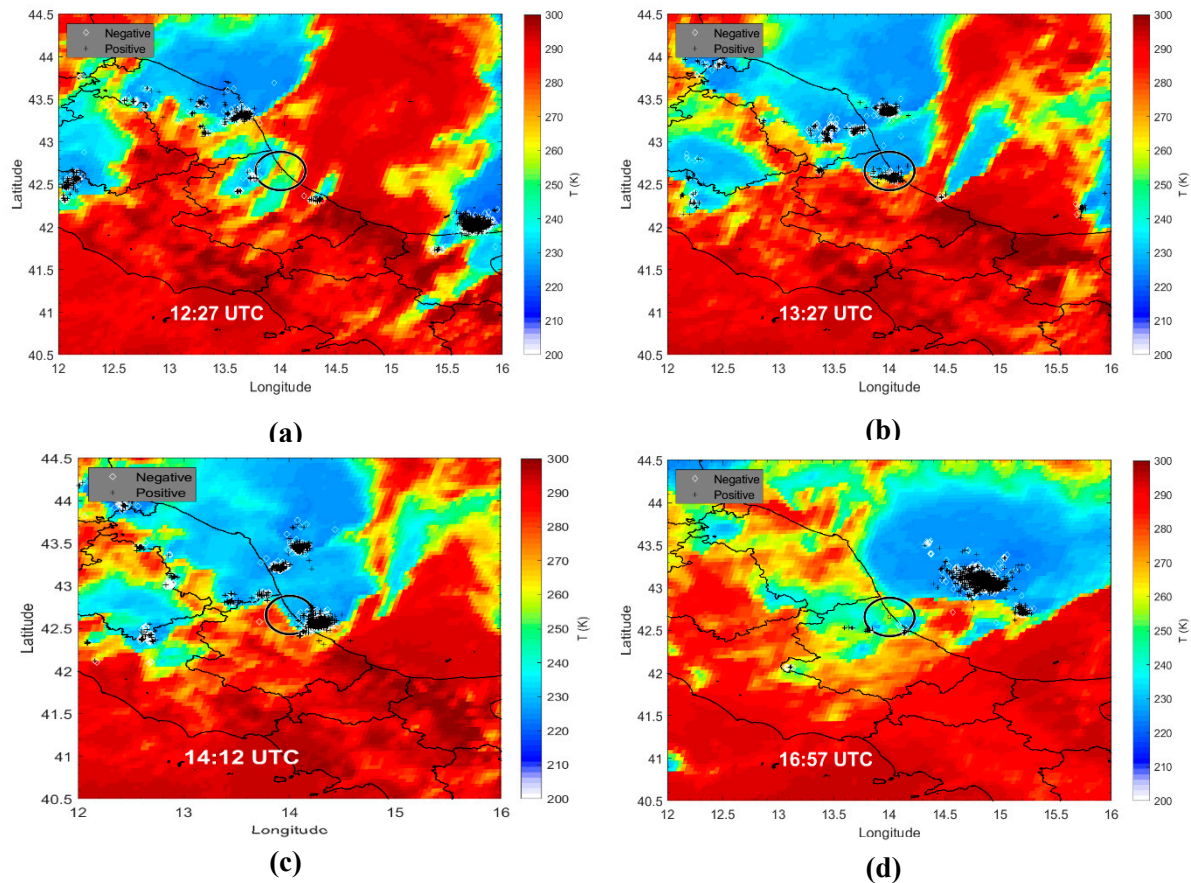


Figure 7. Time evolution of the convective storm, which interested Pineto on 2nd September 2018. The panels (a) to (d) report the TB as measured by SEVIRI channel 9 and the positive (black crosses) and negative (white diamonds) strokes, as recorded by LINET network at (a) 12:27, (b) 13:27, (c) 14:12, and (d) 16:57 UTS, respectively. The black circle is centred in correspondence of GPS antenna and identifies the area where its measurements are consistent (i.e., around a 25-km radius).

Figure 7 is the same as Figure 2 and shows two main differences with respect to the case study of Naples: the storm does not present a single well organized and deep convective cell, and the TB_{ch9} , generally higher than 230 K evidences a limited vertical cloud extension. The precipitative systems developed inland over the Apennines and moved in the south–west/north–east direction. The main lightning activity over the area of measurement (i.e., around the GPS antenna—the black circle in Figure 7—occurred in the early afternoon (Figure 7b–c) when the cloud top of the convective cell drops to about 220 K. At the end of the event between 15:00 and 18:00 UTC, the most intense lightning activity moved over the sea (Figure 7d). As already highlighted in the previous case study (Figure 2), the lightning strokes (both positive and negative) interested the edge of each cell, in the updraft region.

Figure 8 (the same as Figure 3) shows the hourly trend of the IC/CG ratio and the total lightning strokes detected during the storm evaluated over the $1^\circ \times 1^\circ$ box centred on the position of the GPS antenna. Moreover, the vertical grey dashed lines simply identify the time interval of interest (i.e., the time interval when the storm overpassed the measuring site), while the horizontal red dashed line represents the mean value of the IC/CG ratio over the same $1^\circ \times 1^\circ$ box for seven years, from 2012 to 2018.

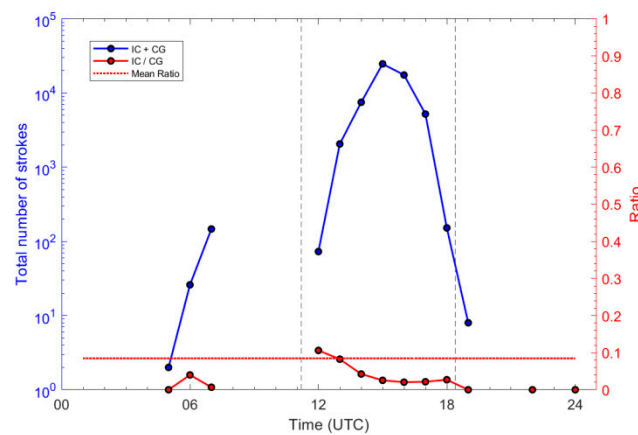


Figure 8. Hourly trend of IC/CG ratio (solid red line) and total number of strokes (blue line) on 2nd September 2018 over a $1^\circ \times 1^\circ$ box centred on the GPS antenna. The horizontal red dashed line represents the mean value of the IC/CG ratio over the same $1^\circ \times 1^\circ$ box for seven years, from 2012 to 2018.

Figure 8 shows that, looking at the time interval limited by the grey dotted vertical lines, the maximum value of the IC/CG ratio (red line) precedes the peak of the maximum number of total lightning strokes (blue line), but has a much less marked trend than the latter. This is due to the low number of IC lightning strokes (compared to the CG) recorded by LINET during the whole event, representing therefore only a small part of the total lightning. It should be noted that the IC/CG ratio, unlike the previous case, is only slightly higher than the seven-year average. The absence of a LINET sensor in the immediate vicinity of Pineto is certainly not conducive to optimal detection of ICs in the area, unlike in the previous case. Apart from this, the IC/CG ratio values at 12:00 and 13:00 UTC refer to the lightning activity that occurred both over land and over sea, while the most intense activity occurred between 14:00 and 17:00 UTC (the main peak reporting almost 25,000 strokes occurred at 15:00 UTC) over sea, approximately 100 km from Pineto, where it is reasonable to assume that the LINET sensitivity in IC detection is lower.

Figure 9 shows the daily trend of PWV (blue line), of TB_{ch9} (red line), of the difference between TB measured by SEVIRI channel 5 and 6 (ΔTB —dotted point light blue line), and of total lightning (black line).

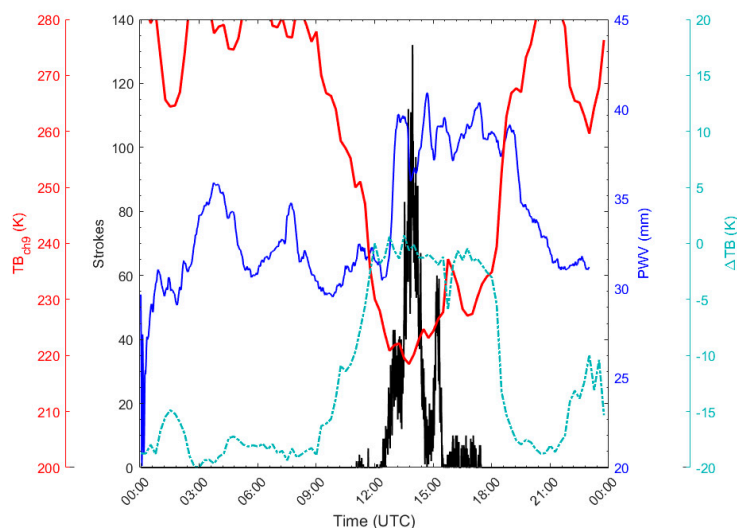


Figure 9. Trend of total number of strokes (black line), PWV (blue line), TB_{ch9} (red line), and ΔTB (dashed sky blue line) for the whole day of 2nd September 2018 over the Pineto area.

Figure 9 shows similar properties to the Naples case study. Both TB_{ch9} and ΔTB start to decrease and increase, respectively, at the same moment (around 09:00 UTC). ΔTB reaches an approximately constant value around 0 K about two hours before the main lightning activity, and this is in good agreement with the results shown in Figure 4. The PWV, as in the Naples case study, shows a rapid and marked increase up to values around 2.52 m once that ΔTB values have reached values close to 0 K. Two other local PWV maxima can be identified at about 03:30 and 07:30 UTC, but they are not associated to high (low) values of ΔTB (TB_{ch9}) or to any lightning activity.

As in the Naples case study, a considerable amount of positive strokes (the 65% of the total recorded strokes) occurred on Pineto during the considered event, while the highest current intensity values were associated with negative strokes (Figure 10). As already highlighted in Figure 5, both positive and negative strokes occurred at a wide range of PWV values (from 30 mm to 41 m, but with higher occurrence for PWV between 36 mm and 41 mm), thus not indicating any direct correlation.

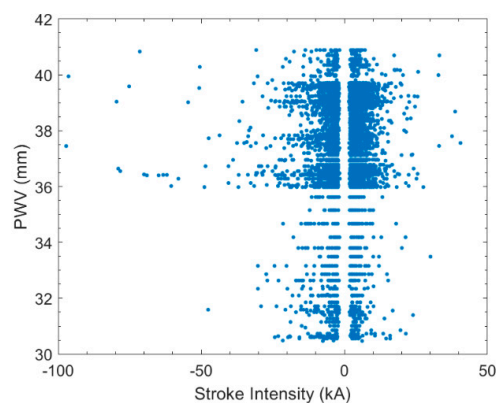


Figure 10. Scatterplot of PWV as a function of strokes intensity.

Also for this case we wanted to consider a scatterplot made to look for a pattern that relates ΔTB , PWV, and the time of occurrence with respect to the main lightning activity. Figure 11 shows a similar pattern with respect to the Naples case study, with the points preceding the main lightning activity reporting ΔTB values greater than 0 K (this is not true for all the points). On the other hand, all the points following the main lightning activity have negative ΔTB values up to -3 K. It is worth noting that the Pineto case study presents different lightning characteristics with respect to the Naples case study, since the main lightning activity is followed by a second local maximum and weak lightning activity lasting for about four hours. This is symptomatic of relevant (in terms of cloud thickness) cloud coverage which does not allow to reach ΔTB values as low as for the Naples case study.

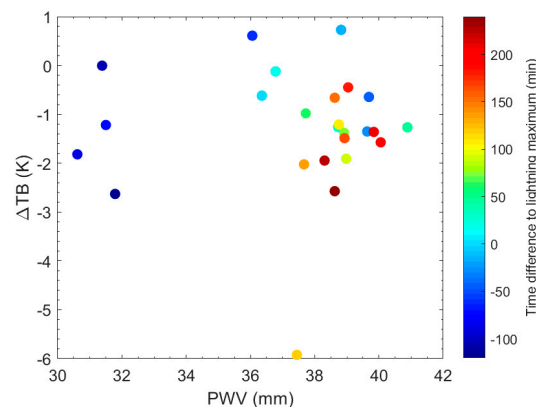


Figure 11. Scatterplot of ΔTB with respect to PWV as a function of time difference with respect to the main lightning activity.

4. Conclusions

The possible relationship among different atmospheric parameters and lightning activity has been investigated by analyzing some convective case studies, two of which are reported and described in this paper. In particular, the PWV coming from the measurements of a GPS antenna, very close to the area where convection develops, and the characteristics of the clouds, as they can be observed from the measurements of the SEVIRI radiometer have been related to the lightning data as obtained from the LINET network. The main idea that led this research was to investigate which precursor signals of the intensification of electrical activity can be expected from satellite data (e.g., SEVIRI data) and/or GPS measurements.

The combination of the parameters mentioned above shows a pattern in both the considered case studies: the lightning activity is generally preceded by a period in which the ΔTB (i.e., the difference between SEVIRI TB at channel 5 and channel 6) presents quite constant values around 0 K (or even positive values), and generally greater than -5 K. When ΔTB reaches this plateau, the PWV starts to increase up to reach a maximum (or a series of maxima) in conjunction with the major lightning activity of the considered event. This mechanism starts to take place about two or three hours before the main lightning activity. This trend is generally confirmed, also considering all the case studies analyzed (not shown), even if a single number quantifying the minimum time interval to predict the main lightning activity is hard to provide. At the same time, the results do not totally clarify if a corresponding PWV threshold could be provided. This is mainly related to the fact that PWV being an integrated measure, it is markedly affected by the meteorological conditions, the season, the location, etc. Furthermore, the results seem to highlight that the combined use of PWV and ΔTB measurements prevents any possible false alarm: local PWV maxima not corresponding to ΔTB increase up to positive values occurred in correspondence of absent lightning activity as well as the opposite is true (i.e., ΔTB values slightly positive or close to zero with low PWV values).

It is worth noting that the two events analyzed even if they show different microphysics properties (the convective cell for the case study of Naples presented very deep vertical extension with very low thermal TB and a well-defined structure with respect to the case study of Pineto), evidence similar characteristics from the lightning activity point of view. For both case studies, the IC/CG ratio was higher than the mean value calculated over seven years in the same area, but presents different magnitudes (going from 0.1 for Pineto up to 2.6 for Naples). The proximity of a LINET sensor to the study area plays a crucial role in the IC detection efficiency. Moreover, the peak of IC/CG ratio precedes the peak of the total lightning activity, which is characterized by a high occurrence (more than 50%) of positive strokes.

The results presented in this paper therefore show the good potential of using radiometer and GPS measurements to predict lightning activity or more generally for use in nowcasting systems. At the same time, it is clear that the present study is an exploratory work that, in order to lead to a robust application result, needs to be contextualized to the territory, through further data and analysis.

Author Contributions: Conceptualization, L.P.D. and S.D.; Methodology, L.P.D. and S.D.; Validation, L.P.; Formal Analysis, L.P. and A.M.; Investigation, L.P.; Resources, S.D.; Data Curation, L.P.D., L.P., and A.M.; Writing—Original Draft Preparation, L.P.D.; Writing—Review and Editing, S.D., A.M., and A.T.; Visualization, L.P.D. and L.P.; Supervision, L.P.D. and S.D. All authors have read and agreed to the published version of the manuscript.

Funding: This research received no external funding.

Acknowledgments: LINET data were provided by Nowcast GmbH (<https://www.nowcast.de/>) within a scientific agreement between Hans Dieter Betz and the Satellite Meteorological Group of CNR-ISAC in Rome.

Conflicts of Interest: The authors declare no conflict of interest.

References

1. Willis, P.T.; Hallett, J.; Black, R.A.; Hendricks, W. An aircraft study of rapid precipitation development and electrification in a growing convective cloud. *Atmos. Res.* **1994**, *33*, 1–24. [[CrossRef](#)]

2. Takahashi, T. Riming Electrification as a Charge Generation Mechanism in Thunderstorms. *J. Atmos. Sci.* **1978**, *35*, 1536–1548. [[CrossRef](#)]
3. Jayaratne, E.R.; Saunders, C.P.R.; Hallett, J. Laboratory studies of the charging of soft-hail during ice crystal interactions. *Q. J. Royal Met. Soc.* **1983**, *109*, 609–630. [[CrossRef](#)]
4. López, R.E.; Aubagnac, J.-P. The lightning activity of a hailstorm as a function of changes in its microphysical characteristics inferred from polarimetric radar observations. *J. Geophys. Res.* **1997**, *102*, 16799–16813. [[CrossRef](#)]
5. Saunders, C.P.R.; Keith, W.D.; Mitzeva, R.P. The effect of liquid water on thunderstorm charging. *J. Geophys. Res.* **1991**, *96*, 11007. [[CrossRef](#)]
6. Figueras i Ventura, J.; Pineda, N.; Besic, N.; Grazioli, J.; Hering, A.; van der Velde, O.A.; Romero, D.; Sunjerga, A.; Mostajabi, A.; Azadifar, M.; et al. Polarimetric radar characteristics of lightning initiation and propagating channels. *Atmos. Meas. Tech.* **2019**, *12*, 2881–2911. [[CrossRef](#)]
7. Figueras i Ventura, J.; Pineda, N.; Besic, N.; Grazioli, J.; Hering, A.; van der Velde, O.A.; Romero, D.; Sunjerga, A.; Mostajabi, A.; Azadifar, M.; et al. Analysis of the lightning production of convective cells. *Atmos. Meas. Tech.* **2019**, *12*, 5573–5591. [[CrossRef](#)]
8. Price, C.; Asfur, M. *Lightning and Climate: The Water Vapor Connection*; American Geophysical Union: Washington, DC, USA, 2001.
9. Bevis, M.; Businger, S.; Herring, T.A.; Rocken, C.; Anthes, R.A.; Ware, R.H. GPS meteorology: Remote sensing of atmospheric water vapor using the global positioning system. *J. Geophys. Res.* **1992**, *97*, 15787. [[CrossRef](#)]
10. Duan, J.; Bevis, M.; Fang, P.; Bock, Y.; Chiswell, S.; Businger, S.; Rocken, C.; Solheim, F.; van Hove, T.; Ware, R.H.; et al. GPS Meteorology: Direct Estimation of the Absolute Value of Precipitable Water. *J. Appl. Meteorol.* **1996**, *35*, 830–838. [[CrossRef](#)]
11. Businger, S.; Chiswell, S.; Bevis, M.; Duan, J.; Anthes, R.A.; Rocken, C.; Ware, R.H.; Exner, M.; van Hove, T.; Solheim, F. The Promise of GPS in Atmospheric Monitoring. *Bull. Am. Meteorol. Soci.* **1996**, *77*, 5–18. [[CrossRef](#)]
12. Sapucci, L.F.; Machado, L.A.T.; Menezes de Souza, E.; Campos, T.B. GPS-PWV jumps before intense rain events. *Atmos. Meas. Tech. Discuss.* **2016**, 1–27. [[CrossRef](#)]
13. Shoji, Y. Retrieval of Water Vapor Inhomogeneity Using the Japanese Nationwide GPS Array and its Potential for Prediction of Convective Precipitation. *J. Meteorol. Soci. Japan* **2013**, *91*, 43–62. [[CrossRef](#)]
14. Realini, E.; Sato, K.; Tsuda, T.; Susilo; Manik, T. An observation campaign of precipitable water vapor with multiple GPS receivers in western Java, Indonesia. *Prog. Earth Planet. Sci.* **2014**, *1*, 17. [[CrossRef](#)]
15. Mascitelli, A.; Federico, S.; Fortunato, M.; Avolio, E.; Torcasio, R.C.; Realini, E.; Mazzoni, A.; Transerici, C.; Crespi, M.; Dietrich, S. Data assimilation of GPS-ZTD into the RAMS model through 3D-Var: Preliminary results at the regional scale. *Meas. Sci. Technol.* **2019**, *30*, 055801. [[CrossRef](#)]
16. Inoue, H.Y.; Inoue, T. Characteristics of the Water-Vapor Field over the Kanto District Associated with Summer Thunderstorm Activities. *SOLA* **2007**, *3*, 101–104. [[CrossRef](#)]
17. Farnell, C.; Rigo, T.; Pineda, N. Lightning jump as a nowcast predictor: Application to severe weather events in Catalonia. *Atmos. Res.* **2017**, *183*, 130–141. [[CrossRef](#)]
18. Schultz, E.; Schultz, C.; Carey, L.; Cecil, D.; Bateman, M. Automated storm tracking and the lightning jump algorithm using GOES-R Geostationary Lightning Mapper (GLM) proxy data. *J. Oper. Meteor.* **2016**, *4*, 92–107. [[CrossRef](#)]
19. Farnell, C.; Rigo, T.; Pineda, N. Exploring radar and lightning variables associated with the Lightning Jump. Can we predict the size of the hail? *Atmos. Res.* **2018**, *202*, 175–186. [[CrossRef](#)]
20. Betz, H.-D.; Schmidt, K.; Oettinger, P.; Wirz, M. Lightning detection with 3-D discrimination of intracloud and cloud-to-ground discharges: LIGHTNING DETECTION WITH 3-D MODE. *Geophys. Res. Lett.* **2004**, *31*. [[CrossRef](#)]
21. Betz, H.-D.; Schmidt, K.; Fuchs, B.; Oettinger, W.P.; Holler, H. Cloud Lightning: Detection and Utilization for Total Lightning Measured in the VLF/LF Regime. *J. Lightning Res.* **2007**, *2*, 1–17.
22. Schmid, J. *The SEVIRI Instrument*; ESA/ESTEC: Noordwijk, The Netherlands, 2000; pp. 13–32.
23. Sampietro, D.; Caldera, S.; Capponi, M.; Realini, E. *Geoguard—An Innovative Technology Based on Low-Cost GNSS Receivers to Monitor Surface Deformations*; European Association of Geoscientists & Engineers: Amsterdam, The Netherlands, 2017.

24. Mascitelli, A.; Coletta, V.; Bombi, P.; de Cinti, B.; Federico, S.; Matteucci, G.; Mazzoni, A.; Muzzini, V.G.; Petenko, I.; Dietrich, S. Tree Motion: Following the wind-induced swaying of arboreous individual using a GNSS receiver. *Ital. J. Agrometeorol.* **2019**, *3*, 25–36.
25. Colosimo, G. *VADASE: Variometric Approach for Displacement Analysis Stand-Alone Engine*; La Sapienza Univ.: Rome, Italy, 2012.
26. Fratarcangeli, F.; Savastano, G.; D’Achille, M.; Mazzoni, A.; Crespi, M.; Riguzzi, F.; Devoti, R.; Pietrantonio, G. VADASE Reliability and Accuracy of Real-Time Displacement Estimation: Application to the Central Italy 2016 Earthquakes. *Remote Sens.* **2018**, *10*, 1201. [[CrossRef](#)]
27. Campanelli, M.; Mascitelli, A.; Sanò, P.; Diémoz, H.; Estellés, V.; Federico, S.; Iannarelli, A.M.; Fratarcangeli, F.; Mazzoni, A.; Realini, E.; et al. Precipitable water vapour content from ESR/SKYNET sun–sky radiometers: Validation against GNSS/GPS and AERONET over three different sites in Europe. *Atmos. Meas. Tech.* **2018**, *11*, 81–94. [[CrossRef](#)]
28. Capponi, M.; Sampietro, D.; Sansò, F. *Very Improved KINematic Gravimetry: A New Approach to Aerogravimetry*; La Sapienza Univ.: Rome, Italy, 2018.
29. Klejer, F. *Troposphere Modeling and Filtering for Precise GPS Leveling*; Publications on Geodesy; Nederlandse Commissie voor Geodesie: Delft, The Netherlands, 2004; ISBN 978-90-6132-284-9.
30. Hofmann-Wellenhof, B.; Lichtenegger, H.; Collins, J. *Global Positioning System: Theory and Practice*; Springer: Wien, Austria, 1992; ISBN 978-3-211-82364-4.
31. Zumberge, J.F.; Heflin, M.B.; Jefferson, D.C.; Watkins, M.M.; Webb, F.H. Precise point positioning for the efficient and robust analysis of GPS data from large networks. *J. Geophys. Res.* **1997**, *102*, 5005–5017. [[CrossRef](#)]
32. Takasu, T.; Yasuda, A. Development of the low-cost RTK-GPS receiver with an open source program package RTKLIB. In Proceedings of the International Convention Center Jeju Korea, Jeju, Korea, 10 December 2009; pp. 4–6.
33. Hersbach, H.; de Rosnay, P.; Bell, B.; Schepers, D.; Simmons, A.; Soci, C.; Abdalla, S.; Alonso-Balmaseda, M.; Balsamo, G.; Bechtold, P.; et al. *Operational Global Reanalysis: Progress, Future Directions and Synergies with NWP*; ERA Report Series; ECMWF: Berkshire, UK, 2018.
34. Berberan-Santos, M.N.; Bodunov, E.N.; Pogliani, L. On the barometric formula. *Am. J. Phys.* **1997**, *65*, 404–412. [[CrossRef](#)]
35. Bai, Z.; Feng, Y. GPS water vapor estimation using interpolated surface meteorological data from Australian automatic weather stations. *J. Global Position. Syst.* **2003**, *2*, 83–89. [[CrossRef](#)]
36. Marra, A.C.; Porcù, F.; Baldini, L.; Petracca, M.; Casella, D.; Dietrich, S.; Mugnai, A.; Sanò, P.; Vulpiani, G.; Panegrossi, G. Observational analysis of an exceptionally intense hailstorm over the Mediterranean area: Role of the GPM Core Observatory. *Atmos. Res.* **2017**, *192*, 72–90. [[CrossRef](#)]

